Acta Pharmaceutica Sinica B 2021;11(5):1300−1314

Chinese Pharmaceutical Association
Institute of Materia Medica, Chinese Academy of Medical Sciences

Acta Pharmaceutica Sinica B

www.elsevier.com/locate/apsb
www.sciencedirect.com

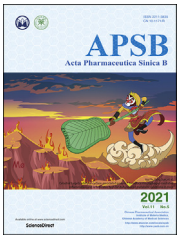

ORIGINAL ARTICLE

Discovery of an orally active VHL-recruiting PROTAC that achieves robust HMGCR degradation and potent hypolipidemic activity *in vivo*

Guoshun Luo[a], Zhenbang Li[a], Xin Lin[a], Xinyu Li[b], Yu Chen[c], Kun Xi[b], Maoxu Xiao[a], Hanlin Wei[a], Lizhe Zhu[b,*], Hua Xiang[a,*]

[a]*State Key Laboratory of Natural Medicines and Department of Medicinal Chemistry, China Pharmaceutical University, Nanjing 211198, China*
[b]*School of Life and Health Sciences and Warshel Institute for Computational Biology, the Chinese University of Hong Kong, Shenzhen 518172, China*
[c]*Key Laboratory of Smart Drug Delivery, Ministry of Education School of Pharmacy, Fudan University, Shanghai 201203, China*

Received 29 August 2020; received in revised form 22 October 2020; accepted 30 October 2020

KEY WORDS

HMGCR;
PROTACs;
Oral bioavailability;
Cholesterol reduction

Abstract HMG-CoA reductase (HMGCR) protein is usually upregulated after statin (HMGCR inhibitor) treatment, which inevitably diminishes its therapeutic efficacy, provoking the need for higher doses associated with adverse effects. The proteolysis targeting chimera (PROTAC) technology has recently emerged as a powerful approach for inducing protein degradation. Nonetheless, due to their bifunctional nature, developing orally bioavailable PROTACs remains a great challenge. Herein, we identified a powerful HMGCR-targeted PROTAC (**21c**) comprising a VHL ligand conjugated to lovastatin acid that potently degrades HMGCR in Insig-silenced HepG2 cells (DC_{50} = 120 nmol/L) and forms a stable ternary complex, as predicated by a holistic modeling protocol. Most importantly, oral administration of the corresponding lactone **21b** reveled favorable plasma exposures referring to both the parent **21b** and the conversed acid **21c**. Further *in vivo* studies of **21b** demonstrated robust HMGCR degradation

Abbreviations: CRBN, cereblon; CVD, cardiovascular disease; DC_{50}, half degradation concentration; ER, endoplasmic reticulum; HDAC, histone deacetylase; HMGCR, 3-hydroxy-3-methylglutaryl coenzyme A reductase; H&E, hematoxylin/eosin; LDL-C, low-density lipoprotein cholesterol; MFD, medium fat diet; ORO, oil-red O; PK, pharmacokinetic; PROTAC, proteolysis-targeting chimera; SAR, structure−activity relationship; TC, total cholesterol; TG, triglyceride; VHL, von Hippel-Lindau.

*Corresponding authors. Tel./fax: +86 755 23519577 (Lizhe Zhu), +86 25 83271096 (Hua Xiang).
E-mail addresses: zhulizhe@cuhk.edu.cn (Lizhe Zhu), xianghua@cpu.edu.cn (Hua Xiang).

Peer review under responsibility of Institute of Materia Medica, Chinese Academy of Medical Sciences and Chinese Pharmaceutical Association.

https://doi.org/10.1016/j.apsb.2020.11.001

and potent cholesterol reduction in mice with diet-induced hypercholesterolemia, highlighting a promising strategy for treating hyperlipidemia and associated diseases.

1. Introduction

Atherogenic dyslipidemia characterized by elevated cholesterol, especially high levels of low-density lipoprotein (LDL) cholesterol, is an important cause of cardiovascular disease (CVD)[1]. Pharmacological management of hypercholesterolemia has represented the most effective therapy for cardiovascular disease prevention[2]. 3-Hydroxy-3-methylglutaryl coenzyme A (HMG-CoA) reductase (HMGCR), a well-established target for hypolipidemic drugs, is the rate-limiting enzyme of the mevalonate pathway, which catalyzes the conversion of HMG-CoA to the key precursor of cholesterol, mevalonate (Fig. 1A)[3–5]. Statins are a class of HMGCR inhibitors with HMG-like moieties that competitively bind to the catalytic site, thereby blocking the production of mevalonate and sterols (Fig. 1A)[5,6]. Owing to their efficacy in reducing plasma cholesterol levels, statins remain as the main therapy for hypercholesterolemia and CVD[7,8]. However, there are concerns regarding poor statin adherence including insufficient dosing and high discontinuation rates, which have been documented in approximately fifty percent of patients[9–12]. Particularly, inhibiting HMGCR function by statins usually leads to a compensatory upregulation of HMGCR protein (Fig. 1A), which has been observed in both research models[13–15] and humans[16] and is believed to unavoidably hamper the effectiveness of statins and limit their clinical applications[17–19].

HMGCR is an endoplasmic reticulum (ER)-localized transmembrane protein whose amount under physiological conditions is regulated through multiple feedback mechanisms[4,20,21]. On the one hand, reduction of cholesterol synthesis activates the sterol-regulatory element binding protein (SREBP) pathway, leading to augmentation of HMGCR gene transcription[4]. On the other hand, less production of cholesterol and downstream intermediates maintains HMGCR protein stabilization by blocking the sterol-induced ubiquitination of HMGCR[22–24], a native process of Insig-mediated HMGCR degradation[25,26]. Regarding statin-induced HMGCR increment, reduced HMGCR degradation was recently recognized as the predominant mechanism (Fig. 1A)[27]. indicating that ablating both activity and abundance of HMGCR would be a new and promising strategy to lower cholesterol levels.

As a novel chemical knockdown technology, proteolysis-targeting chimera (PROTAC)[28–30] has recently emerged as a promising approach with potential to address the limitations of conventional drug development paradigms[31–35]. PROTACs are bifunctional compounds consisting of two independent ligands connected by a chemical linker, with one ligand specifically binding to target protein and the other ligand recruiting an E3 ubiquitin ligase. Upon ternary complex formation, the target protein is polyubiquitinated and subsequently degraded by the proteasome[36]. While this rapidly developed technique has been widely employed in the degradation of various oncogenic proteins[37–40], its application in CVD, the leading cause of global deaths, remains relatively less explored[41]. Moreover, examples of PROTACs with potent *in vivo* activity and favorable pharmacokinetic (PK) properties are scarce[42], with most administered *via* injection rather than *via* the oral route[43–45]. Inspired by the native Insig-mediated degradation process, we envisioned a feasible way

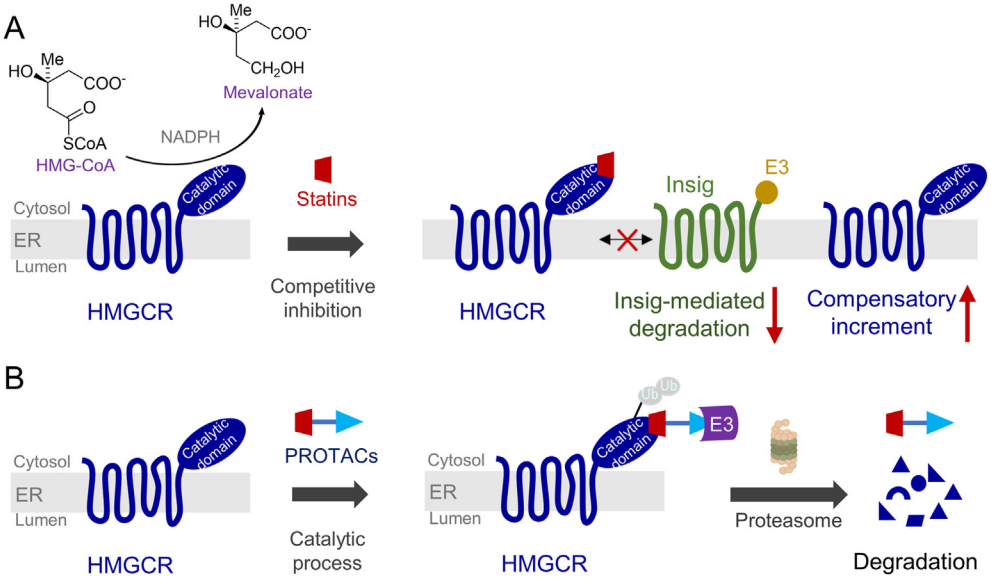

Figure 1 (A) HMGCR inhibition by statins leads to the compensatory upregulation of HMGCR. (B) Illustration of PROTAC-mediated HMGCR degradation.

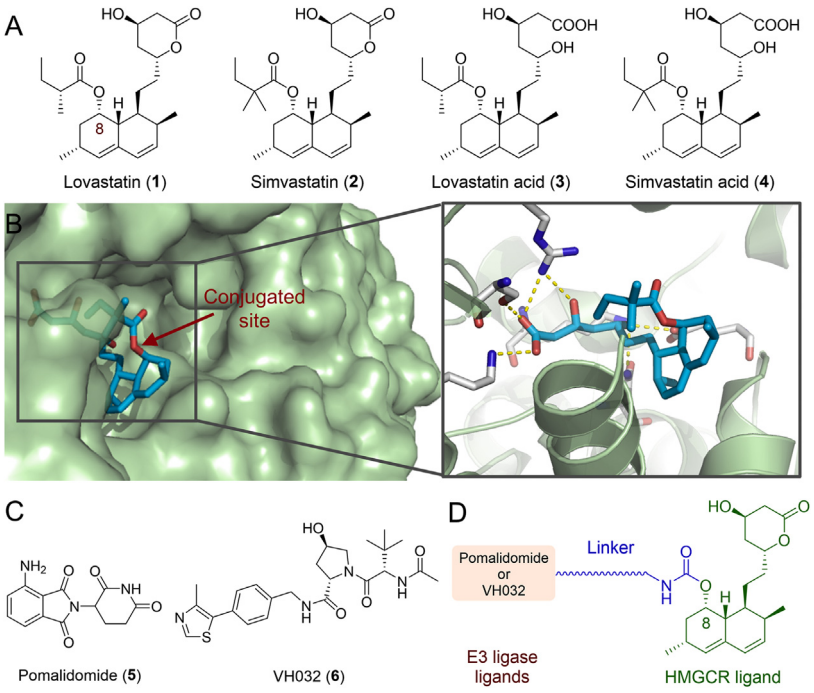

Figure 2 (A) Structures of the HMGCR inhibitors lovastatin (**1**) and simvastatin (**2**) together with their active forms (**3** and **4**). (B) Cocrystal structure of HMGCR catalytic domain complexed with simvastatin acid (**4**) (PDB: 1HW9). The conjugated site is indicated by a red arrow. (C) Structures of the E3 ligase ligands pomalidomide (**5**) and VH032 (**6**). (D) A general scheme for the design of HMGCR-targeting PROTAC probes.

to eliminate HMGCR by using artificial conjugates (HMGCR-targeting PROTACs) that hijack different E3 ligases such as von Hippel-Lindau (VHL) and CRBN (Fig. 1B).

Herein, we describe the development of various HMGCR-targeted PROTACs by connecting lovastatin with either CRBN ligand pomalidomide or VHL ligand VHL231. While our work was underway, Rao group[46] revealed a comprehensive structure−activity relationship (SAR) analysis of atorvastatin−CRBN conjugates, confirming that the ER-localized membrane protein HMGCR can be successfully degraded *in vitro* by CRBN−proteasome system. Nevertheless, attempts to validate its therapeutic efficacy *in vivo* need to be conducted. Furthermore, pursuing orally bioavailable PROTACs, albeit highly challenging, is of great significance particularly for hyperlipidemia, a chronic disease that usually requires long-term medication. Encouragingly, we identified a potent VHL-based PROTAC **21c** that induces profound HMGCR degradation in Insig-silenced HepG2 cells through a VHL-dependent manner, a process that was further confirmed by the formation of a stable PROTAC-mediated ternary complex during *in silico* modeling. Most importantly, the corresponding lactone prodrug **21b** has shown to afford high plasma exposures referring to the active ingredient **21c**, leading to efficient HMGCR degradation and promising cholesterol-lowering potency *in vivo*. Overall, our work identified a first-generation, orally active VHL-based degrader of HMGCR, and proved that inducing the degradation of HMGCR by PROTACs can potently reduce cholesterol levels, providing a new strategy to prevent CVD.

2. Results and discussion

2.1. *Design, synthesis, and preliminary biological evaluation*

HMGCR-targeting PROTACs were designed based on the first-generation HMGCR inhibitors lovastatin/simvastatin (Fig. 2A), orally bioavailable prodrugs that are transformed to the corresponding β-hydroxyacids (active forms **3** or **4**, Fig. 2A) after oral ingestion. The cocrystal structure of simvastatin acid (**3**) bound to HMGCR[5] revealed that the crucial β-hydroxyacid moiety formed hydrogen bonds with key residues in the HMG-CoA pocket (Fig. 2B). The 8-butyrate not involved in any interactions with HMGCR was identified as a solvent exposed group, which has been verified by a previously developed dual HMGCR/HDAC inhibitor where the hydroxamic acid was attached *via* a carbamate linker to the C-8 oxygen atom of lovastatin[47]. These results indicated that the 8-butyrate of lovastatin/simvastatin may be a suitable site for the attachment of E3 ligase ligands (Fig. 2B). To probe the potential degradation of ER membrane-bound HMGCR by artificial PROTAC conjugates, the CRBN ligand pomalidomide (**5**) and the VHL ligand VH032 (**6**, Fig. 2C), two widely used E3 ligase-recruiting moieties, were examined in this study. Thus, we initially designed several HMGCR-targeting PROTAC probes by connecting E3 ligase ligands to the C-8 position of lovastatin through various carbamate linkers (Fig. 2D).

The preparation of designed compounds **16a–16c** was outlined in Scheme 1. Compound **9** was synthesized through four steps according to a previously reported route[47]. Treatment of the commercially available lovastatin with KOH in H_2O/MeOH concurrently led to the production of ester-cleaved and lactone-opened intermediate, which was directly converted to its lactone form **7** under acidic conditions (6 mol/L HCl). Selective protection of the less-hindered hydroxyl group with a bulky TBS group provided compound **8**, which subsequently reacted with *p*-nitrophenyl chloroformate to produce the key intermediate **9**. Condensation of compound **9** with pomalidomide analogs **14a–14c**, which were synthesized according to previously published procedures[48], yielded compounds **15a–15c**. Further deprotection of the TBS group led to the final CRBN-based PROTACs **16a–16c**. Similarly, as depicted in Scheme 2, the VHL-based

PROTACs **21a** and **21b** were prepared by the condensation of the key intermediate **9** with VH032 analogs **19a** and **19b**[49].

According to previous studies[47], lovastatin derivatives bearing linear substitutions at the C-8 position showed HMGCR inhibition that is comparable to lovastatin. Therefore, to confirm the retention of HMGCR catalytic domain binding, the inhibitory activities of synthetic compounds on HMGCR were initially examined by a cell-free enzymatic assay. As expected, conjugating the E3 recruiting ligand at C-8 position of lovastatin does not have a major effect on HMGCR inhibition. All compounds presented low micromolar potency with IC_{50} values (1.25−2.49 μmol/L) comparable to that of lovastatin (0.74 μmol/L, Table 1 and Supporting Information Fig. S1), implying that these 8-*O*-linked analogs maintained reasonable affinity for HMGCR.

We then performed Western blot analyses to assess the ability of these analogs to prevent the compensatory upregulation of HMGCR in human hepatic HepG2 cells. As is shown in Fig. 3, consistent with previous findings[27] that statins slow the native degradation of HMGCR leading to its increment, and treatment of lovastatin at a range of concentrations for 16 h remarkably upregulated HMGCR in a dose-dependent manner. In contrast, we were pleased to find that both the CRBN- and VHL-based compounds effectively attenuated the compensatory upregulation of HMGCR (Fig. 3) at a nontoxic concentration of 1 μmol/L, as measured by Cell-Counting Kit-8 assay (Supporting Information Fig. S2). Although native Insig-mediated HMGCR degradation might have disrupted the results, our data obtained by directly comparing PROTAC-treated groups with untreated controls under the same conditions (Fig. 3) clearly indicated that these compounds induced HMGCR degradation to a further extent. Compound **16b**, possessing an ethylene glycol linker, was the most potent among the CRBN-based PROTACs, with 56% protein remaining relative to the untreated control, while the long carbon chain-linked VHL analog **21b** exerted the most potent efficacy with 42% protein remaining (Table 1). Despite limited SAR analysis results, we reasoned that ER-bound HMGCR can be degraded by PROTACs hijacking ether the CRBN or VHL E3 ligase. However, several limitations of CRBN-based PROTACs have been previously reported including the intrinsic activity of the CRBN ligand on non-PROTAC targets and chemical instability[48]. The latter was also observed in CRBN-based compound **16b** that showed over half decomposition in silane at 37 °C after 24 h (Supporting Information Fig. S3). With the aim of identifying a PROTAC suitable for *in vivo* studies, we turned our attention, therefore, to VHL-based PROTACs.

These lovastatin-derived PROTACs in the lactone form, albeit with acceptable HMGCR inhibition and degradation, were in fact prodrugs, which may produce different cellular actions. To further investigate the prodrug characteristics, we next prepared PROTAC **21c** (Fig. 4A), the lactone-opened form of **21b**, which in terms of the hydroxy acid pharmacophore is predicted to have better affinity for HMGCR. As expected, **21c** demonstrated improved HMGCR inhibition with an IC_{50} value of 0.25 μmol/L (Fig. 4A). We then established dose−response protein curves for **21c** and its parent lactone **21b** for comparison (Fig. 4B and C). At lower doses, both PROTAC **21b** and **21c** attenuated the upregulation of HMGCR. Whereas higher concentrations lead to an increase in HMGCR expression, referred as the characteristic "hook effect", indicating that these PROTACs preferentially act as HMGCR inhibitors over degraders at high doses. Additionally, another plausible explanation may be that, as HMGCR inhibition gradually dominated (particularly for **21c**, Fig. 4C), greater HMGCR accumulation caused by the hindered Insig-pathway might have offset the effect of PROTACs. These results preliminarily indicated that **21c** was able to inhibit HMGCR activity through the lovatstain acid moiety while promoting HMGCR degradation

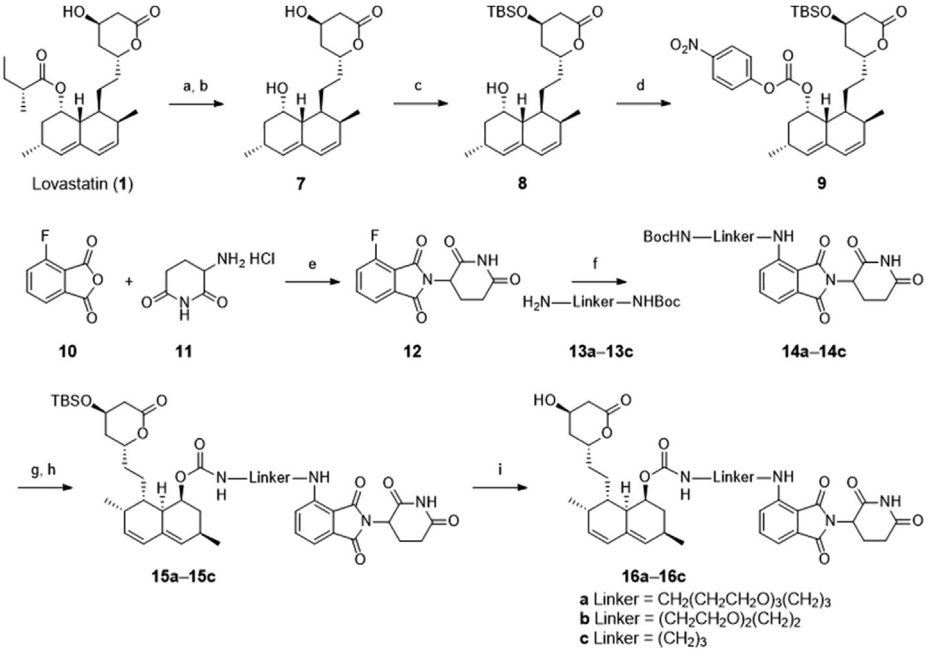

Scheme 1 Synthesis of the CRBN-based compounds **16a–16c**. Reagents and conditions: (a) KOH, H_2O/MeOH, reflux, 12 h; (b) 6 mol/L HCl, rt, 6 h, 45% obtained in two steps; (c) TBSCl, imidazole, CH_2Cl_2, rt, 6 h, 84%; (d) *p*-nitrophenyl chloroformate, DMAP, pyridine, rt, 16 h, 64%; (e) NaOAc, AcOH, 12 h, reflux, 70%; (f) *N*,*N*-diisopropylethylamine, DMF, 90 °C, 12 h, 35%−45%; (g) TFA, DCM, rt, 0.5 h; (h) **9**, DMAP, pyridine, rt, 16 h, 60%−75%; (i) $BF_3 \cdot OEt_2$, MeCN, 0 °C, 0.5 h, 52%−65%.

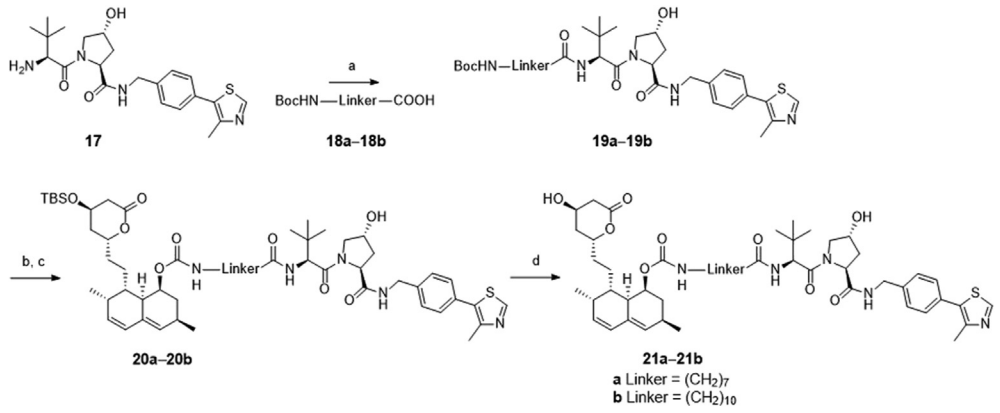

Scheme 2 Synthesis of VHL-based compounds **21a** and **21b**. Reagents and conditions: (a) *N*,*N*-diisopropylethylamine, HATU, DMF, rt, 12 h, 35−55%; (b) TFA, DCM, rt, 0.5 h; (c) **9**, DMAP, pyridine, rt, 16 h, 45%−65%; (d) $BF_3 \cdot OEt_2$, MeCN, 0 °C, 0.5 h, 55%−60%.

Table 1 HMGCR-targeted PROTACs derived from lovastatin with pomalidomide or VH032.

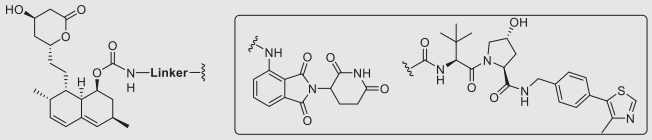

Compd.	Linker	E3 ligase	HMGCR inhibition IC_{50} (μmol/L)[a]	Remaining HMGCR at 1 μmol/L (%)[b]
16a	$CH_2(CH_2CH_2O)_3(CH_2)_3$	CRBN	1.25	73 ± 6
16b	$(CH_2CH_2O)_2(CH_2)_2$	CRBN	1.88	56 ± 4
16c	$(CH_2)_3$	CRBN	2.49	89 ± 7
21a	$(CH_2)_7$	VHL	1.56	63 ± 5
21b	$(CH_2)_{10}$	VHL	1.32	42 ± 5
Lovastatin	−	−	0.74	266 ± 29

[a]IC_{50} values for HMGCR inhibition were obtained from triplicate experiments.
[b]Percentage HMGCR level remaining relative to the control of each compound at 1 μmol/L. The data are the means ± SD from three independent experiments. − Not applicable.

through the VHL moiety. Compared to the lactone **21b**, which achieved a maximum degradation (D_{max}) of 56% at a high dose of 1 μmol/L, the corresponding acid **21c** was more efficient in inducing HMGCR degradation (D_{max} = 65%, at 0.1 μmol/L). Further evaluation of lovastatin, **21b** and **21c** under the same conditions confirmed that **21c** was a promising HMGCR degrader capable of reducing cellular cholesterol (Supporting Information Fig. S5), which was thus selected for further cellular mechanism studies.

2.2. *Validation of PROTAC (**21c**)-mediated HMGCR degradation in Insig-silenced HepG2 cells*

As mentioned above, statin-induced upregulation of HMGCR was recently shown to be primarily the result of HMGCR stabilization, as the interaction between HMGCR and Insig, as well as the subsequent ubiquitination and degradation, were blocked. To exclude inherent Insig-mediated effect on HMGCR expression, we used siRNA to knockdown Insig-1 and Insig-2 in HepG2 cells (Fig. 5A) that expressed constant HMGCR levels regardless of statin treatment (Fig. 5B), allowing the direct and specific assessment of PROTAC-triggered HMGCR degradation[46]. First, HMGCR degradation by varying concentrations of PROTAC **21c** was evaluated to assess the DC_{50} (concentration causing 50% HMGCR degradation). As shown in Fig. 5C, **21c** effectively degraded the HMGCR protein with a DC_{50} of 0.12 μmol/L, and achieved a D_{max} of 76% at 1 μmol/L, confirming that **21c** induces PROTAC-mediated HMGCR degradation. As observed in wide-type HepG2 cells, elevated HMGCR expression was also observed in the Insig-silenced HepG2 cells at higher concentration of 3 μmol/L. However, this "hook effect" is mainly attributed to the PROTAC characteristics rather than the combinational feedback effects shown in Fig. 4C. Furthermore, a time-course study revealed that compound **21c** reduced HMGCR protein level in a time-dependent manner (Supporting Information Fig. S6).

To further explore the mechanism of **21c**-induced HMGCR degradation, we treated Insig-silenced HepG2 cells with **21c**, the VHL ligand (VHL032) and the proteasome inhibitor MG-132 in various concentrations. As shown in Fig. 5D, HMGCR degradation induced by **21c** at 1 μmol/L was significantly blocked by the addition of VHL032 (10 μmol/L) or MG132 (10 μmol/L). Moreover, addition of lovastatin (3 μmol/L) also efficiently reduced **21c**-induced HMGCR degradation (Fig. 5E). All these mechanistic data confirmed that PROTAC **21c** bound simultaneously to HMGCR and VHL, and subsequently degraded HMGCR by the VHL-dependent ubiquitin−proteasome system.

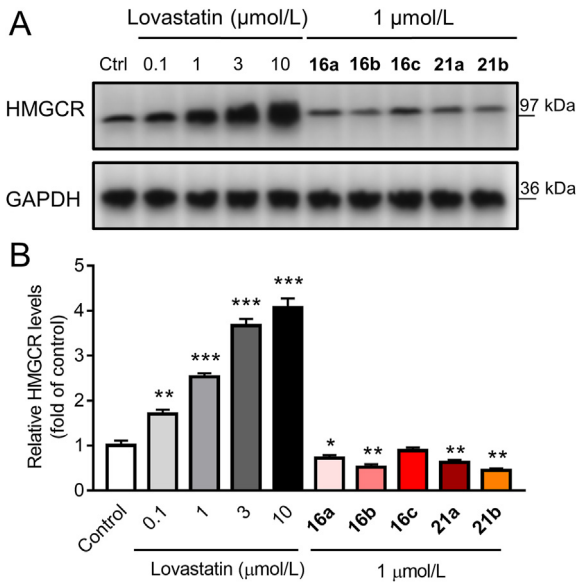

Figure 3 Effect of lovastatin and PROTACs on HMGCR expression in HepG2 cells. (A) Cells were treated with DMSO, lovastatin (0.1, 1, 3 and 10 μmol/L) or compounds **16a–16c**, or **21a–21b** (1 μmol/L) for 16 h. Original blots are shown in Supporting Information Fig. S4. The data are represented as fold change relative to the control, means ± SD ($n = 3$). *$P < 0.05$, **$P < 0.01$, ***$P < 0.001$ *vs*. DMSO-control.

2.3. *In silico modeling of the PROTAC (**21c**)-mediated ternary complex*

The formation of a favorable ternary complex induced by a PROTAC is considered paramount for valid degradation. To elucidate the potential ternary complex formation between **21c**, HMGCR and VHL, we conducted *in silico* modeling, an attractive surrogate for *in vitro* experiments, using a holistic protocol[50,51] including several consecutive steps described in detail in Supporting Information Fig. S7. Initially, the Rosetta protein−protein docking framework[52] was used to build a global HMGCR−VHL interaction modes. Among them, the decoy with packstat score ≥0.5 and binding energy ≤−1.0 (Fig. 6A) was selected to further generate ternary complexes through linker conformer alignment, which outputs a set of feasible ternary modes (Fig. 6B). Then, the pose with the lowest protein docking score and ligand conformer energy (the one in the blue circle, Fig. 6C) was advanced for a 500 ns molecular dynamics simulation to verify whether it could maintain a stable ternary conformation. As is shown in Fig. 6D and E, the conformation ensemble can be separated into three parts with initial steady state lasting through approximately 100 frames (10 ns), a second state lasting from 100 to 800 frames, and the last conformation stabilizing during the rest of the simulation time, which clearly indicated a stable ternary conformation (3rd state, named HMGCR−**21c**−VHL_3). A detailed analysis revealed that the β-hydroxyacid moiety of **21c** fit well into the catalytic pocket of HMGCR forming hydrogen bonds with key residues, and the

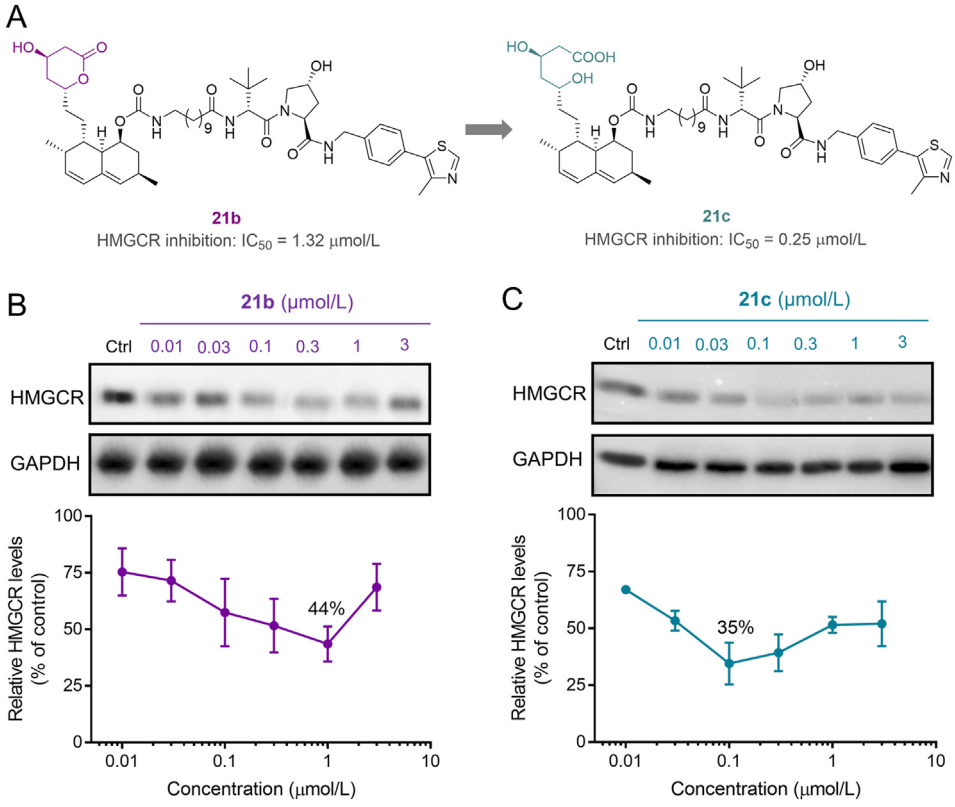

Figure 4 Comparison of the lactone **21b** to the corresponding acid **21c** in enzymatic and cellular assays. (A) Hydrolysis of the lactone ring to generate the ring-opened acid **21c** with improved HMGCR inhibition. (B) and (C) HepG2 cells treated with **21b** or **21c** at indicated doses for 16 h, were analyzed for protein levels. The data are represented as %HMGCR remaining relative to the DMSO-control (defined as 100%), and presented as the mean ± SD from two repeated experiments shown in Fig. S4.

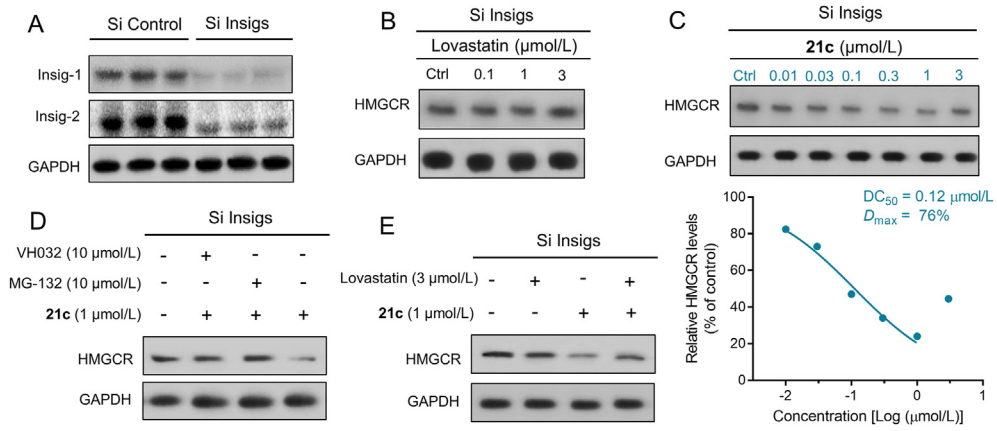

Figure 5 Compound **21c** induces HMGCR degradation through VHL-dependent ubiquitin−proteasome system in Insig-silenced HepG2 cells. (A) Knockdown efficiency of Insig-1 and Insig-2 in HepG2 cells was determined by Western blotting. (B) and (C) Insig-silenced HepG2 cells treated with lovastatin or **21c** at the indicated doses (16 h), were examined. (D) and (E) Cells pretreated for 6 h with VH032 (10 μmol/L), the proteasome inhibitor MG-132 (10 μmol/L), lovastatin (3 μmol/L) or DMSO, were subsequently treated for 10 h with compound **21c** (1 μmol/L).

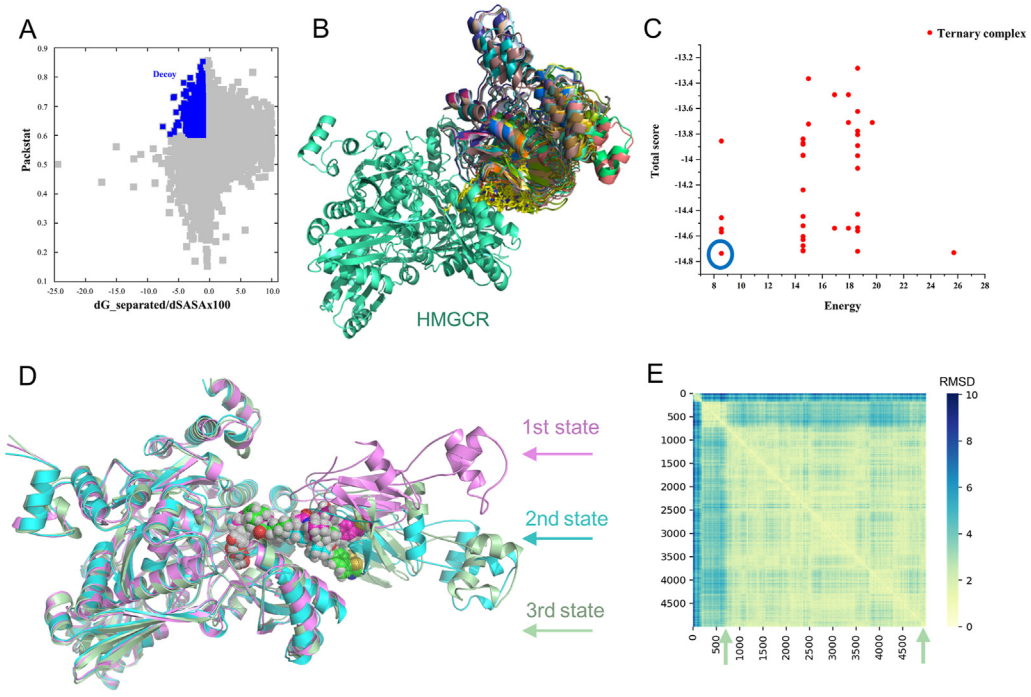

Figure 6 Representative modeling results. (A) Symmetric protein−protein docking energy and packstat score landscape for the interaction between the HMGCR−simvastatin acid complex (PDB: 1HW9) and the VHL−VH032 complex (PDB: 4W9H) through Rosetta docking. The decoy (packstat score ≥0.5 and binding energy ≤−1.0) is shown in blue as insert. (B) Superposition of the ternary mode output after linker conformer alignment. HMGCR, VHL and **21c** poses are shown in green, multicolor and yellow, respectively. (C) Symmetric docking score and ligand conformer energy landscape for the ternary mode output. The pose with the lowest score and energy was selected, as indicated by the blue circle. (D) A 500 ns molecular dynamics simulation of the selected ternary complex revealed three relatively stable HMGCR/**21c**/VHL states, shown as violet (1st state), bright blue (2nd state) and green (3rd state) cartoons, respectively, with **21c** are shown as spheres. (E) Symmetric pair RMSD value landscape of the above three states generated from the 500 ns molecular dynamics simulation. The third state stabilized during the rest of the simulation time (from 800 to 5000 frames) was selected as the most stable conformation (named HMGCR−**21c**−VHL_3) and was used for further analysis.

VH032 moiety engaged the catalytic tunnel of VHL (Fig. 7A and B). In addition, VHL interacted with the catalytic domain of HMGCR, generating an interface area of 1142.525 Å^2 (Fig. 7A). Taken together, these modeling results indicated that **21c** can form a stable ternary conformation with HMGCR and VHL, and their interactions closely resembled those observed in the respective crystal structures (Fig. 7C). Furthermore, these results establish compound **21c** as a suitable VHL-recruiting PROTAC targeting HMGCR for degradation, providing structural insights into the mechanism of PAOTAC (**21c**)-mediated degradation that can

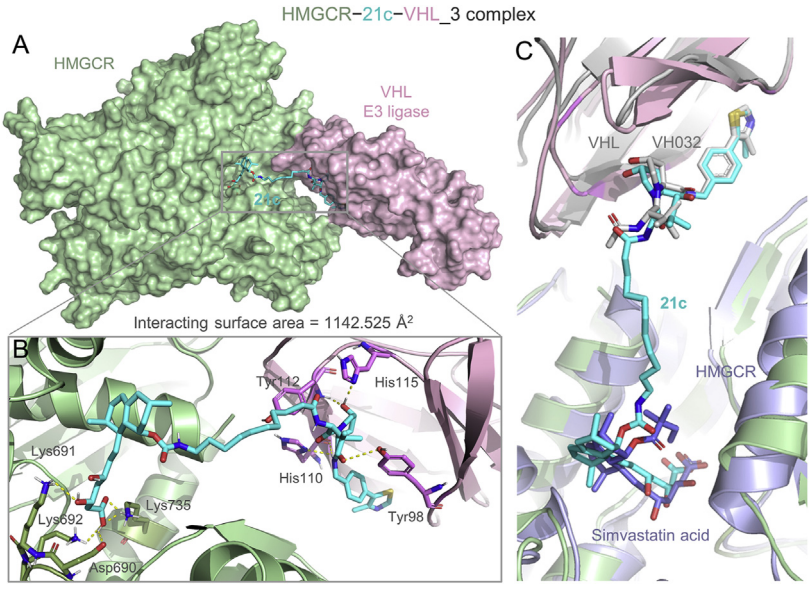

Figure 7 Structure of the most stable model (3rd state, named HMGCR−**21c**−VHL_3) from molecular dynamics simulation of HMGCR/**21c**/VHL ternary complexes is shown. (A) Surface representation of the HMGCR−**21c**−VHL_3 ternary complex: HMGCR (green), VHL (violet) and **21c** (blue stick). (B) Close-up of interactions between HMGCR (green cartoon), VHL (violet cartoon) and **21c** (blue stick). Yellow dotted lines represent H-bond interactions. (C) Superposition of HMGCR−**21c**−VHL_3 complex with the VHL E3 ligase (gray cartoon) bound to VH032 (gray stick) (PDB: 4W9H) and HMGCR (light blue cartoon) bound to simvastatin acid (light blue stick) (PDB: 1HW9).

Table 2 *In vitro* metabolic stability of **21b**, **21c** and lovastatin in mouse liver microsomes.

Compd.	$t_{1/2}$ (min)[a]	CL_{int} (mL/min/kg)[a]
Lovastatin	0.73	7516
21b	4.18	415.81
21c	87.5	62.37

[a]The data are mean of duplicate. Additional data are shown in the Supporting Information Table S21 and Fig. S8.

facilitate further optimization. Additionally, we also performed molecular modeling of the shortest linker containing compound **16c** within HMGCR (PDB: 1HW9) and CRBN (PDB: 4CI3), which failed to provide any ternary complex due to the limit of linker length. Thus, we speculated that the weak degradation of HMGCR by **16c** might be mediated by other mechanisms that needs further investigations.

2.4. *Pharmacokinetic (PK) studies*

Initially, the *in vitro* metabolic stability of lovastatin **21b** and **21c** was evaluated in mouse liver microsomes. As is shown in Table 2, possibly due to the unstable esters (8-butyrate and lactone), lovastatin was metabolized quickly with an extremely high clearance rate. The introduction of the carbamate-linked VHL ligand remarkably enhanced the metabolic stability, with the lactone-opening compound **21c** being the least susceptible to phase I metabolism. Calculation (Supporting Information Table S1), however, suggested that the lactone **21b** has better permeability and intestinal absorption than **21c** and would be less problematic in terms of oral delivery. Furthermore, as lovastatin is an orally bioavailable prodrug, we sought to directly compare the *in vivo* potency of HMGCR inhibitor with that of a degrader; therefore, we selected the lactone form PROTAC **21b** for the following *in vivo* studies. To verify whether oral administration of **21b** can achieve a therapeutically effective concentration, we then conducted pharmacokinetic studies of **21b** in mice and analyzed the PK parameters of both **21b** and its ring-opening metabolite **21c**. Surprisingly, a single oral dosing of **21b** at 60 mg/kg afforded good drug exposure in plasma, resulting in desirable C_{max} and AUC values for both the parent **21b** and active ingredient **21c** (Table 3). Furthermore, the plasma levels of **21b** and its metabolite **21c** reached maximum concentrations after 8 and 4 h (time to peak concentration, T_{max}), respectively, which are longer than those of lovastatin and lovastatin acid previously reported in mice (T_{max} = 2 and 1.5 h, respectively)[53]. Consistent with *in vitro* metabolic stability, **21b** exhibited a slower clearance rate than lovastatin[53] in mice. These encouraging observations indicated that prodrug **21b**, albeit non-adherence to

Table 3 Pharmacokinetic profile of **21b** and metabolite **21c** in mice.

PK parameter	**21b** at 60 mg/kg *p.o.*[a]	
	21b[b]	**21c**[c]
$t_{1/2}$ (h)	5.1 ± 0.4	6.2 ± 0.6
T_{max} (h)	8.0	4.0
C_{max} (μmol/L)	0.47 ± 0.04	0.29 ± 0.03
AUC_{0-24} (μmol·h/L)	5.0 ± 0.41	3.3 ± 0.16
$AUC_{0-\infty}$ (μmol·h/L)	5.4 ± 0.47	3.6 ± 0.18

[a]Prodrug **21b** was dosed *via* a single *p.o.* route at indicated concentrations.
[b]PK parameters of the parent **21b**.
[c]PK parameters of the metabolite **21c**. All data are mean ± SD, n = 5. Additional data are shown in the Supporting Information Fig. S9 and Table S3.

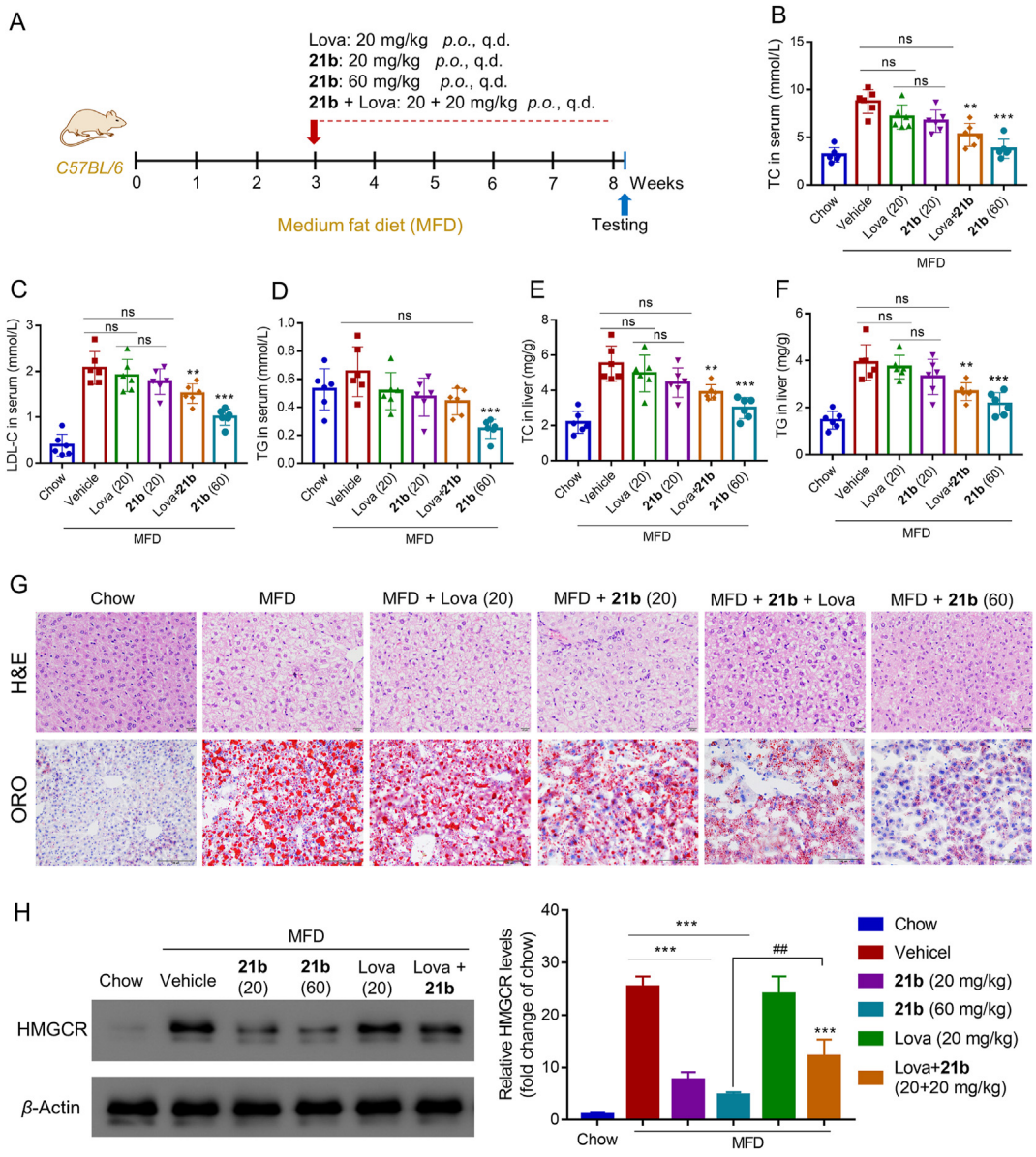

Figure 8 Compound **21b** effectively degraded HMGCR and lowered cholesterol in mice with MFD-induced hypercholesterolemia. (A) Schematic representation of the experimental protocol. C57BL/6 male mice ($n = 6$) on a normal diet or MFD were orally administered lovastatin (20 mg/kg/day), **21b** (20 or 60 mg/kg/day) or combination of **21b** and lovastatin (20 + 20 mg/kg) for 5 weeks. Sixteen hours after the final gavage, livers and plasma were collected and analyzed for serum total cholesterol (TC) (B), serum LDL-C (C), serum TG (D), hepatic TC (E) and hepatic TG (F). Data are the means ± SD ($n = 6$), $^{**}P < 0.01$, $^{***}P < 0.001$ *vs.* untreated MFD vehicle. (G) Photomicrograph of livers stained with H&E (scale bar, 20 μm) and oil red O (ORO) (scale bar, 100 μm). (H) Hepatic HMGCR levels were examined through Western blot experiment. Data are presented as HMGCR fold relative to the chow-control (defined as 1), and as the means ± SD (3 mice per group, Supporting Information Fig. S10), $^{***}P < 0.001$ *vs.* untreated MFD vehicle; $^{\#\#}P < 0.01$ (**21b** group *vs.* **21b**/lovastatin cotreatment group).

the classic "Rule of Five" (Table S1), exhibited favorable absorption properties and oral bioavailability[44], allowing it to be deployed in mouse disease models.

2.5. *In vivo efficacy of compound **21b** in mice with MFD-Induced hypercholesterolemia*

Encouraged by the pharmacokinetic data, we evaluated the effect of compound **21b** on a medium fat diet (MFD)-induced mouse model of hypercholesterolemia. After a 3-week induction of hypercholesterolemia, compound **21b** and lovastatin were administered orally once a day for 5 weeks (Fig. 8A). Notably, compound **21b** was well tolerated, with body weight and food intake comparable to those of the mice treated with lovastatin or MFD vehicle (Supporting Information Fig. S10). As depicted in Fig. 8B–D, compound **21b** at a single oral dose of 20 mg/kg demonstrated similar effects to lovastatin, leading to a moderate decrease of total cholesterol (TC), LDL-C and triglyceride (TG) in serum of mice fed on MFD. Combinations of **21b** and lovastatin enhanced the reduction in serum lipid levels. Moreover, this cholesterol-lowering activity was dose-dependent for **21b**: at a higher dose of 60 mg/kg, serum TC and cholesteryl esters were all significantly reduced to lower levels. Consistently, compound **21b** reduced hepatic TC and TG in a dose-dependent manner (Fig. 8E and F), and ameliorated

MFD-induced steatosis and lipid deposition in liver sections, as determined by histochemical staining (Fig. 8G).

To further clarify the mechanism of **21b**, Western blotting was performed to determine the HMGCR expression in liver. As shown in Fig. 8H, robust HMGCR degradation was induced by **21b** at 16 h after final gavage even at a low dose of 20 mg/kg, while lovastatin group retained high HMGCR level. These findings demonstrate that **21b** is a highly potent and orally active HMGCR degrader. In consistent with above cellular results, addition of lovastatin to **21b** significantly impaired its HMGCR degradation ($^{\#\#}P < 0.01$). It is worth noting that cotreatment of **21b** with lovastatin, albeit attenuating HMGCR degradation, was more effective in lowering total lipids (TC, cholesteryl ester and TG) than respective single drug group. These results suggest that although **21b** at a low dose alone was able to suppress *de novo* cholesterol synthesis *via* HMGCR degradation, synergetic statin therapy and HMGCR degradation may provide greater benefit for promoting excretion of redundant lipids absorbed daily from an MFD[27]. Therefore, considering the pleiotropic effects of statin therapy in the lipid metabolism, combining **21b** with statins could be a potential strategy to produce optimal therapeutic effect that warrants further investigations using respective other kinds of statins and *in vivo* models.

3. Conclusions

The use of PROTACs, as an emerging small-molecule knockdown strategy, has gained considerable attention in both academia and the pharmaceutical industry as means of expanding therapeutic landscapes not accessible to conventional drugs[31–35]. To date, this rapidly developed technique has been successfully employed for the degradation of various proteins involved in cancer[37–40] and neurodegenerative diseases[54,55], including nuclear receptors[56,57], kinases[58–60], epigenetic readers[61–63] and transcription factors[64]. On the other hand, statin-induced compensatory upregulation of HMGCR (an ER transmembrane protein), a common phenomenon[13–16], decreases statin sensitivity and leads to higher dose requirements that unavoidably cause high risks of side effects[17,18]. Fueled by recent progress in accelerating Insig-mediated HMGCR degradation as a potential strategy[27], we sought to probe HMGCR degradation by artificial PROTACs that hijack different E3 ligases, which would be an extension of PROTAC to less-explored cardiovascular diseases.

Lovastatin, an orally bioavailable prodrug, was selected as the HMGCR-recognizing ligand since a previous study confirmed that liner substitutions at the C-8 position maintained HMGCR binding for inhibition[47], making it a reasonable choice for conjugating E3 ligase ligands at this site. Initial screens with HepG2 cells led to VHL-based **21b** as a potent PROTAC achieving the least remaining HMGCR. However, since the HMGCR level is physiologically regulated by Insig-mediated degradation and because blockade of this degradation is the predominant cause of statin-induced HMGCR increment, the results from wide-type HepG2 cells might not truly reflect the potency of PROTAC-mediated degradation, particularly for the acid **21c**, as indicated by more protein remaining at higher treatment concentrations. A plausible explanation might be that HMGCR degradation induced by **21c** *via* the VHL moiety was compromised by HMGCR increment induced by **21c** *via* the lovastatin acid moiety. Subsequent evaluation in Insig-silenced cells, a suitable model for evaluating PROTAC-mediated degradation[46], provided unbiased evidence that **21c** does promote HMGCR degradation *via* the VHL-dependent ubiquitin−proteasome system. Nevertheless, due to this harsh requirement for an Insig-deficient cell model, extensive screens and systematic SAR studies would be impeded. Therefore, we used a combined computational method to evaluate the suitability of **21c** for stable ternary complex formation, providing structural insights to facilitate further optimization.

To directly compare PROTAC with lovastatin, we then selected the lactone form **21b** for further animal studies, which achieved surprisingly good oral PK properties for both parent **21b** and active ingredient **21c**, translating to efficient HMGCR degradation in mice with MFD-induced hypercholesterolemia. The safety profile of **21b** was confirmed when no apparent change of body weight and food intake after long-term treatment (5 weeks). Collectively, as the first-generation VHL-based HMGCR-PROTAC, **21b** has already displayed favorable oral bioavailability and great promise for promoting HMGCR degradation and cholesterol reduction *in vivo*, and can be a promising strategy alone or synergetic with statin therapy for the treatment of hyperlipidemia. Moreover, advances in this work demonstrate that favorable oral PK properties for PROTACs with challenging physicochemical property can be regularly achievable[44], which paves the way for the development of more orally bioavailable PROTACs in the future.

4. Experimental

4.1. Chemistry

Reactions monitorization was conducted by precoated silica gel plates (GF/UV 254) under UV light. To obtain purified compounds, silica gel column (200−300 mesh) was used. EI-MS was collected on Shimadzu GCMS-2010 instruments. High resolution mass spectra (HRMS) were determined by Agilent Technologies 6520 Accurate-Mass Q-TOF MS instruments. Bruker Avance 400 MHz spectrometer was used to determine ^{1}H NMR and ^{13}C NMR. Tetramethylsilane (TMS) was employed as an internal standard. Purity was determined by HPLC: Discovery® 504971 column (C18, 250 mm × 4.6 mm, 5 μm); temperature, 25 °C; injection volume, 5 μL; isocratic flow, rate, 1 mL/min; solvent, 90% MeCN in H_2O, and the purity of target compounds are greater than 95%. Synthesis of intermediate **9** and **15a–15c** are shown in the Supporting Information.

4.1.1. *(1S,3R,7S,8S,8aR)-8-(2-((2R,4R)-4-Hydroxy-6-oxotetrahydro-2H-pyran-2-yl)ethyl)-3,7-dimethyl-1,2,3,7,8,8a-hexahydronaphthalen-1-yl (3-(2-(2-(3-((2-(2,6-dioxopiperidin-3-yl)-1,3-dioxoisoindolin-4-yl)amino)propoxy)ethoxy)ethoxy) propyl)carbamate (**16a**)*

Compound **15a** (0.17 g, 0.18 mmol) in anhydrous CH_3CN was added boron trifluoride etherate (0.031 mL, 0.22 mmol) at 0 °C, and continue to stir for 30 min. After completion, the reaction group was washed with saturated Na_2CO_3 solution, and extracted with EA, then purified through column chromatography to give green solid **16a** (0.076 g, 52% yield). ^{1}H NMR (400 MHz, $CDCl_3$) δ 8.97 (d, J = 3.2 Hz, 1H), 7.53−7.38 (m, 1H), 7.06 (d, J = 7.1 Hz, 1H), 6.92 (d, J = 8.6 Hz, 1H), 6.46 (d, J = 4.9 Hz, 1H), 5.94 (d, J = 9.6 Hz, 1H), 5.76 (dd, J = 9.3, 6.1 Hz, 1H), 5.49 (s, 1H), 5.23 (d, J = 32.2 Hz, 1H), 4.92 (dd, J = 9.7, 5.4 Hz, 1H), 4.61 (d, J = 3.2 Hz, 1H), 4.29 (s, 1H), 3.78−3.31 (m, 15H), 3.24 (d, J = 6.0 Hz, 2H), 2.92−2.28 (m, 7H), 2.23 (d, J = 11.2 Hz, 1H), 2.10 (d, J = 7.0 Hz, 1H), 2.01−1.50 (m, 11H), 1.34 (d, J = 8.7 Hz, 1H), 1.06 (d, J = 7.4 Hz, 3H), 0.87 (d, J = 6.9 Hz, 3H). ^{13}C NMR (101 MHz, $CDCl_3$) δ 171.7, 170.9,

169.4, 167.8, 156.6, 146.9, 136.1, 133.4, 132.5, 131.9, 129.7, 128.3, 116.7, 111.3, 109.8, 70.5, 70.1, 69.2, 68.9, 68.5, 62.3, 60.4, 59.7, 53.5, 48.8, 40.2, 38.5, 37.3, 36.7, 36.1, 32.8, 32.6, 31.4, 30.9, 29.7, 29.2, 27.4, 23.8, 22.8, 22.7, 13.9. MS (ESI) *m/z*: 823.1 $[M+H]^+$. HRMS (ESI): *m/z*, Calcd. for $C_{43}H_{58}N_4O_{12}$ $[M+H]^+$, 823.4131, Found 823.4131. Compounds **16b** and **16c** were synthesized by similar procedure.

*4.1.2. (1S,3R,7S,8S,8aR)-8-(2-((2R,4R)-4-Hydroxy-6-oxotetrahydro-2H-pyran-2-yl)ethyl)-3,7-dimethyl-1,2,3,7,8,8a-hexahydronaphthalen-1-yl (2-(2-(2-((2-(2,6-dioxopiperidin-3-yl)-1,3-dioxoisoindolin-4-yl)amino)ethoxy)ethoxy)ethyl)carbamate (**16b**)*

Yellow solid (0.08 g, 60% yield). ^{1}H NMR (400 MHz, $CDCl_3$) δ 7.50 (t, J = 8.0 Hz, 1H), 7.12 (d, J = 5.6 Hz, 1H), 6.89 (d, J = 8.5 Hz, 1H), 6.52 (s, 1H), 5.96 (d, J = 9.5 Hz, 1H), 5.78 (dd, J = 9.5, 4.8 Hz, 1H), 5.51 (s, 1H), 5.24 (s, 2H), 4.93 (s, 1H), 4.60 (d, J = 23.0 Hz, 1H), 4.27 (m, 1H), 3.80−2.99 (m, 14H), 2.93−2.08 (m, 10H), 2.01−1.48 (m, 9H), 1.34 (dd, J = 25.9, 17.4 Hz, 3H), 1.07 (d, J = 7.3 Hz, 3H), 0.88 (d, J = 4.1 Hz, 3H). ^{13}C NMR (101 MHz, $CDCl_3$) δ 170.7, 169.4, 167.7, 146.7, 136.2, 133.6, 132.6, 131.8, 129.7, 128.2, 116.8, 111.8, 77.4, 77.2, 77.0, 76.7, 76.3, 70.8, 70.3, 69.2, 69.0, 68.8, 62.6, 53.5, 50.2, 48.8, 42.2, 40.8, 38.4, 37.3, 36.8, 32.7, 31.3, 30.9, 29.6, 29.3, 27.4, 23.9, 23.0, 22.7, 13.9, 1.0, 0.01. HRMS (ESI): *m/z*, Calcd. for $C_{39}H_{50}N_4O_{11}$ $[M+H]^+$, 751.3551, Found 751.3554.

*4.1.3. (1S,3R,7S,8S,8aR)-8-(2-((2R,4R)-4-Hydroxy-6-oxotetrahydro-2H-pyran-2-yl)ethyl)-3,7-dimethyl-1,2,3,7,8,8a-hexahydronaphthalen-1-yl (3-((2-(2,6-dioxopiperidin-3-yl)-1,3-dioxoisoindolin-4-yl)amino)propyl)carbamate (**16c**)*

Yellow solid (0.06 g, 65% yield). ^{1}H NMR (400 MHz, $CDCl_3$) δ 9.18 (s, 1H), 7.46 (m, 1H), 7.06 (dd, J = 7.0, 2.4 Hz, 1H), 6.86 (d, J = 8.6 Hz, 1H), 6.43 (s, 1H), 5.96 (d, J = 9.8 Hz, 1H), 5.83−5.58 (m, 1H), 5.51 (s, 1H), 5.36−5.13 (m, 2H), 5.01−4.83 (m, 1H), 4.61 (s, 1H), 4.24 (s, 1H), 3.50 (s, 1H), 3.29 (s, 4H), 2.92−2.68 (m, 3H), 2.60 (dt, J = 29.7, 11.2 Hz, 2H), 2.47−2.16 (m, 4H), 2.09 (s, 1H), 1.77 (m, 8H), 1.44−1.29 (m, 2H), 1.07 (d, J = 7.3 Hz, 3H), 0.88 (m, 3H). ^{13}C NMR (101 MHz, CDCl3) δ 172.1, 171.2, 169.4, 169.3, 167.7, 156.9, 146.7, 136.2, 133.5, 132.5, 132.0, 129.7, 128.3, 116.6, 111.5, 109.9, 75.8, 68.9, 62.4, 60.4, 48.9, 39.6, 38.5, 37.3, 35.9, 32.6, 31.4, 30.9, 29.6, 27.4, 22.7, 21.1, 14.2, 13.9. HRMS (ESI): *m/z*, Calcd. for $C_{36}H_{44}N_4O_9$ $[M+H]^+$, 677.3109, Found 677.3183.

*4.1.4. tert-Butyl (8-(((S)-1-((2S,4R)-4-hydroxy-2-((4-(4-methylthiazol-5-yl)benzyl)carbamoyl)pyrrolidin-1-yl)-3,3-dimethyl-1-oxobutan-2-yl)amino)-8-oxooctyl)carbamate (**19a**)*

Compound **17** (0.4 g) was added to a solution of compound **18a** (0.93 mmol), HATU (0.35 g, 0.93 mmol) and DIEA (1.86 mmol) in 10 mL DMF at rt and stirred for another 12 h. After completion, reaction was washed with H_2O and extracted with EA. Purified by column to afford compound **19a** as a gray solid (0.22 g, 35% yield). MS (ESI) *m/z*: 672.1 $[M+H]^+$. Compound **19b** was synthesized according to the step for **19a**.

*4.1.5. tert-Butyl (11-(((S)-1-((2S,4R)-4-hydroxy-2-((4-(4-methylthiazol-5-yl)benzyl)carbamoyl)pyrrolidin-1-yl)-3,3-dimethyl-1-oxobutan-2-yl)amino)-11-oxoundecyl)carbamate (**19b**)*

Gray solid (1.8 g, 55% yield). MS (ESI) *m/z*: 714.1 $[M+H]^+$.

*4.1.6. (1S,3R,7S,8S,8aR)-8-(2-((2R,4R)-4-((tert-Butyldimethylsilyl)oxy)-6-oxotetrahydro-2H-pyran-2-yl)ethyl)-3,7-dimethyl-1,2,3,7,8,8a-hexahydronaphthalen-1-yl (8-(((S)-1-((2S,4R)-4-hydroxy-2-((4-(4-methylthiazol-5-yl)benzyl)carbamoyl)pyrrolidin-1-yl)-3,3-dimethyl-1-oxobutan-2-yl)amino)-8-oxooctyl)carbamate (**20a**)*

To a solution of carbamate **19a** (0.22 g, 0.33 mmol) in 4 mL DCM was added 2 mL TFA, which was stirred for 30 min at rt. After evaporation, the resultant crude was dissolved in anhydrous pyridine (2 mL), and was added carbonate **9** (0.09 g, 0.15 mmol), and DMAP (0.07 g, 0.6 mmol). The reaction was stirred at rt for 16 h. After completion, pyridine was removed, and the residue was extracted with EA and washed with 1 mol/L HCl, dried by anhydrous Na_2SO_4, and then purified by column using CH_2Cl_2/MeOH to give white solid **20a** (0.1 g). MS (ESI) *m/z*: 1032.1 $[M+H]^+$. Compounds **20b** (white solid, 45% yield). MS (ESI) *m/z*: 1074.1 $[M+H]^+$ was obtained according to the step for **20a**.

*4.1.7. (1S,3R,7S,8S,8aR)-8-(2-((2R,4R)-4-Hydroxy-6-oxotetrahydro-2H-pyran-2-yl)ethyl)-3,7-dimethyl-1,2,3,7,8,8a-hexahydronaphthalen-1-yl (8-(((S)-1-((2S,4R)-4-hydroxy-2-((4-(4-methylthiazol-5-yl)benzyl)carbamoyl)pyrrolidin-1-yl)-3,3-dimethyl-1-oxobutan-2-yl)amino)-8-oxooctyl)carbamate (**21a**)*

According to the synthesis of **16a**, compound **21a** was obtained as a white solid (55% yield). ^{1}H NMR (400 MHz, $CDCl_3$) δ 8.68 (s, 1H), 7.55 (d, J = 5.0 Hz, 1H), 7.35 (s, 4H), 6.49 (d, J = 9.0 Hz, 1H), 5.95 (d, J = 9.7 Hz, 1H), 5.84−5.67 (m, 1H), 5.49 (s, 1H), 5.18 (s, 1H), 4.98 (s, 1H), 4.74−4.45 (m, 6H), 4.43−4.19 (m, 3H), 4.01 (d, J = 11.1 Hz, 1H), 3.65 (d, J = 13.5 Hz, 1H), 3.25−2.93 (m, 2H), 2.67 (dd, J = 23.2, 18.1 Hz, 4H), 2.50 (s, 3H), 2.45−2.28 (m, 3H), 2.20 (t, J = 16.2 Hz, 4H), 1.85 (dd, J = 37.6, 30.5 Hz, 4H), 1.75−1.48 (m, 5H), 1.47−1.11 (m, 13H), 1.06−0.91 (m, 12H), 0.87 (d, J = 7.0 Hz, 4H). ^{13}C NMR (101 MHz, $CDCl_3$) δ 174.0, 171.2, 156.6, 150.43, 148.3, 138.3, 133.5, 131.9, 131.7, 130.8, 130.7, 129.7, 129.4, 128.0, 76.2, 69.9, 68.5, 62.5, 60.4, 58.9, 57.5, 56.9, 43.1, 40.7, 38.6, 37.3, 36.7, 36.2, 36.1, 35.4, 33.1, 32.6, 30.9, 29.8, 28.5, 27.4, 26.4, 26.1, 25.4, 23.9, 22.7, 21.1, 16.0, 14.2, 13.9. HRMS (ESI): *m/z*, Calcd. for $C_{50}H_{71}N_5O_9S$ $[M+H]^+$, 918.5045, Found 918.5048.

*4.1.8. (1S,3R,7S,8S,8aR)-8-(2-((2R,4R)-4-Hydroxy-6-oxotetrahydro-2H-pyran-2-yl)ethyl)-3,7-dimethyl-1,2,3,7,8,8a-hexahydronaphthalen-1-yl (11-(((S)-1-((2S,4R)-4-hydroxy-2-((4-(4-methylthiazol-5-yl)benzyl)carbamoyl)pyrrolidin-1-yl)-3,3-dimethyl-1-oxobutan-2-yl)amino)-11-oxoundecyl)carbamate (**21b**)*

According to the synthesis of **16a**, compound **21b** was obtained as a white solid (0.19 g, 60% yield). ^{1}H NMR (400 MHz, $CDCl_3$) δ 8.66 (s, 1H), 7.56 (s, 1H), 7.33 (s, 4H), 6.45 (d, J = 8.6 Hz, 1H), 5.94 (d, J = 9.7 Hz, 1H), 5.75 (dd, J = 9.2, 6.2 Hz, 1H), 5.48 (s, 1H), 5.16 (s, 1H), 4.99 (s, 1H), 4.57 (ddd, J = 21.5, 15.6, 6.8 Hz, 6H), 4.37−4.19 (m, 3H), 3.99 (d, J = 11.1 Hz, 1H), 3.65 (d, J = 7.8 Hz, 1H), 3.09 (d, J = 6.2 Hz, 2H), 2.63 (d, J = 3.7 Hz, 2H), 2.48 (s, 3H), 2.43−2.04 (m, 7H), 1.97 (s, 1H), 1.80 (d, J = 9.2 Hz, 2H), 1.74−1.47 (m, 5H), 1.36 (m, 4H), 1.29−1.15 (m, 14H), 0.94 (s, 8H), 0.86 (d, J = 6.8 Hz, 4H). ^{13}C NMR (101 MHz, $CDCl_3$) δ 173.8, 171.5, 171.3, 171.2, 156.6, 150.5, 148.3, 138.3, 133.4, 131.93, 131.7, 130.7, 129.7, 129.4, 128.2, 127.9, 77.3, 76.4, 69.9, 68.4, 62.2, 60.4, 58.9, 57.4, 56.9, 43.1, 40.8, 38.7, 37.3, 36.6, 36.4, 35.9, 35.4, 32.9, 32.7, 30.9, 29.9, 29.2, 29.0, 27.4, 26.5, 26.4, 25.6, 23.8, 22.7, 21.1, 16.0, 14.12, 13.9. HRMS (ESI): *m/z*, Calcd. for $C_{53}H_{77}N_5O_9S$ $[M+H]^+$, 960.5509, Found 960.5514.

*4.1.9. (3R)-3,5-Dihydroxy-7-((1S,2S,6R,8S,8aR)-8-(((5-(((S)-1-((2S,4R)-4-hydroxy-2-((4-(4-methylthiazol-5-yl)benzyl) carbamoyl)pyrrolidin-1-yl)-3,3-dimethyl-1-oxobutan-2-yl)amino)-5-oxopentyl)carbamoyl)oxy)-2,6-dimethyl-1,2,6,7,8,8a-hexahydronaphthalen-1-yl)heptanoic acid (**21c**)*

Compound **21b** (40 mg, 0.04 mmol) was dissolved in THF/H_2O (0.5 mL/0.5 mL), LiOH (1 mg, 0.04 mmol) was added, then the mixture was stirred at rt for 0.5 h. Purification using preparative TLC chromatography provided compound **21c** as a white solid (24 mg, 60% yield). ^{1}H NMR (400 MHz, DMSO) δ 8.98 (d, J = 6.1 Hz, 1H), 8.62−8.50 (m, 1H), 7.81 (t, J = 9.7 Hz, 1H), 7.53−7.34 (m, 5H), 6.90 (d, J = 20.0 Hz, 1H), 5.89 (t, J = 12.5 Hz, 1H), 5.76 (dd, J = 20.3, 11.0 Hz, 1H), 5.43 (d, J = 18.0 Hz, 1H), 5.36−5.27 (m, 1H), 5.03 (s, 1H), 4.53 (t, J = 12.1 Hz, 1H), 4.48−4.32 (m, 4H), 4.30−4.18 (m, 1H), 3.99 (s, 1H), 3.72−3.61 (m, 5H), 3.00−2.84 (m, 2H), 2.45 (s, 5H), 2.41−2.14 (m, 11H), 2.14−1.95 (m, 14H), 1.95−1.77 (m, 13H), 1.64 (s, 1H), 1.54−1.39 (m, 8H), 1.35 (d, J = 8.7 Hz, 5H), 1.04 (d, J = 7.1 Hz, 6H), 0.85 (dd, J = 16.5, 6.6 Hz, 9H). ^{13}C NMR (101 MHz, DMSO) δ 172.6, 170.2, 151.9, 148.2, 146.7, 139.9, 132.6, 131.6, 130.1, 129.7, 129.1, 128.7, 127.9, 70.3, 69.3, 66.6, 59.2, 56.8, 44.8, 43.1, 42.1, 38.4, 37.4, 36.4, 35.7, 35.6, 35.4, 35.1, 32.7, 31.7, 31.6, 30.9, 30.3, 29.9, 29.5, 29.5, 29.4, 29.4, 29.3, 29.3, 29.3, 29.2, 29.0, 27.5, 27.0, 26.8, 26.6, 25.9, 25.6, 24.5, 22.8, 22.54, 16.4, 14.4, 14.3. HRMS (ESI): m/z, Calcd. for $C_{53}H_{79}N_5O_{10}S$ $[M+H]^+$, 978.5620, Found 978.5626.

4.2. Pharmacology

4.2.1. HMG-CoA reductase activity assay

The inhibition of indicated compounds on HMGCR activity was evaluated by the HMGCR kit according to manufacturer's instructions with minor modifications (Biovision, Catalog # K588-100). Briefly, lovastatin or test compounds (5 μL) dissolved in DMSO were incubated with recombinant HMGCR protein (2 μL) in assay buffer at rt for 10 min, then HMG-CoA (5 μL), NADPH (2 μL) were added, then the mix was incubated for 10 min in water bath (37 °C). The absorbance was detected using a Multiskan Sky (Thermo Scientific), fitted with a 340 nm excitation filter. Sample absorbance was measured against a blank, containing no HMGCR. The IC_{50} values for the test compounds were calculated using Graphpad Prism software.

4.2.2. Cell culture

Human hepatic HepG2 cells purchased from ATCC (MD, USA) were maintained in EMEM (Gibco, NY, USA) that contains 10% FBS (fetal bovine serum, Gibco), 100 μg/mL streptomycin sulfate and 100 units/mL penicillin (Sigma, St. Louis, MO, USA). Si-HepG2 cells (Insig-1 and Insig-2 silenced HepG2 cells) were self-made and maintained in DMEM (Gibco C11995500BT) with 10% FBS (Gibco), 100 μg/mL streptomycin sulfate and 100 units/mL penicillin.

4.2.3. Insig-1 and Insig-2 knockdown

Sequence information of siRNA duplexes used in this work are shown in the following: siRNA-Insig-1 (sc-44432, Santa Cruz), 5′-AGGACGACAGTTAGCTATGGGTG-3′; siRNA-Insig-2 (sc-45781, Santa Cruz), 5′-GGCUUUCACUUAAGAACUUTT-3′; NC-siRNA, 5′-UUCUCCGAACGUGUCACGUTT-3′. According to the manufacturer's protocols of Lipofectamine RNAimax (11668-0194, Invitrogen), the siRNA sequences of respective duplexes were transfected into HepG2 and incubated for 48 h, then analyzed by immunoblotting.

4.2.4. Western blotting assay

Cells plated into 6- or 12-well plates were treated with indicated compounds at varying doses. Whole cell lysates were collected by RIPA Lysis Buffer (Solarbio) with protease inhibitor. The determination of protein concentrations was conducted by BCA assay (Beyotime), Equal cell lysates were electrophoresed through 10% SDS-polyacrylamide gels and transferred onto polyvinylidene difluoride membranes and blotted against different target antibodies at 4 °C overnight. Primary antibodies include Anti-HMGCR (ab174830, Abcam), Anti-Insig-1 (ab112248, Abcam) and Anti-Insig-2 (ab86145, Abcam).

4.2.5. Cellular cholesterol assay

Cellular cholesterol content in HepG2 cells was determined using Amplex Red Cholesterol Assay Kit (Invitrogen, Catalog No. A12216), according to the manufacturer's instructions. Briefly, HepG2 cells seeded in 12-well plates were incubated with tested compounds for 24 h. Cellular free cholesterol were extracted with lysis buffer, the mixture was then centrifuged (2000×g, 5 min), and the supernatant was added to glass tube containing working liquid for the cholesterol assay. Free cholesterol is oxidized by cholesterol oxidase to yield hydrogen peroxide that then reacts with Amplex Red reagent to produce fluorescent resorufin, which is measured in a fluorescence microplate reader at 550 nm (excitation) and 590 nm (emission).

4.2.6. Ternary complex modeling

Protein−protein docking were performed by Rosetta software suite (www.rosettacommons.org)[50]. RDKit, an open-source cheminformatics software, version 2030.03, was employed to generate conformers. To model the ternary structure for HMGCR, VHL and PROTAC, co-structures (HMGCR−simvastatin complex: 1HW9 and VHL−VH032 complex: 4W9H) were downloaded from PDB. Rosetta docking_protocol.mpi_linuxgccrelease program was used to generate 10,000 initial protein−protein interaction results which were then analyzed by InterfaceAnalyzer.mpi.linuxgccrelease. RDKit was used to generate 10,000 linker conformations with threshold value larger than 1.5. The code used in RDKi is shown in attached file: Linker conformation generator.py. Then, a custom python script was employed to predict ternary models through RMSD values. Finally, kinetics of selected ternary complex were evaluated by molecular dynamics simulation. Detailed computational methods and procedures are detailed in Supporting Information.

4.2.7. In vitro metabolic stability assay

The metabolic stability assay in mouse liver microsomes was conducted in Shanghai ChemPartner Co., Ltd. (Shanghai, China) with the approval from Animal Committee of Shanghai ChemPartner Co., Ltd. The assay incubation system contained microsomes (0.5 mg/mL, Corning), test compounds (1 μmol/L) and NADPH regeneration system (6 mmol/L) in phosphate buffer (1.0 mmol/L EDTA) at pH 7.4. Then 15 μL of NADPH stock solution (6 mmol/L) was added to the plates to start the reaction. At 5, 15, 30, and 45 min, 135 μL of ACN containing internal standard was added, respectively, to stop the reaction. The mixture was shaken on the vibrator (IKA, MTS 2/4) for 10 min (600 rpm) and then centrifuged at 5594×g for 15 min (Thermo Multifuge × 3R). Transfer 50 μL of the supernatant from each

well into a 96-well sample plate containing 50 μL of ultra pure water (Millipore, ZMQS50F01) for LC−MS/MS analysis.

4.2.8. Animals

For pharmacokinetic studies, C57BL/6 mice were purchased from Hangzhou Subsource Experimental Animal Technology Co., Ltd. (SCXK: 2019-0004, Hangzhou, China). For hypercholesterolemia models, male C57BL/6 mice (20−24 g) were obtained from Nanjing Qinglongshan Animal Company (Nanjing, China). Mice were maintained under standard conditions with *ad libitum* access to water. In the study of hypercholesterolemia, C57BL/6 mice were fed with MFD (medium-fat containing 12% fat, 0.5% sodium cholate and 1.25% cholesterol) for 8 weeks. Mice were handled with the approval from Animal Committee of China Pharmaceutical University, Nanjing, China.

4.2.9. Pharmacokinetic studies

Compound **21b** was dissolved in saline containing 0.5% CMC-Na and given orally at a single dose of 60 mg/kg ($n = 5$ per group, two groups), respectively; three animals received the vehicle (saline containing 5% CMC-Na). After administration, blood samples (50 μL/time) were collected *via* the lateral vein at different times (first group at 0.25, 0.5, 1, and 2 h; second group at 4, 8, 12, and 24 h). The blood samples were mixed with 20 μL internal standard and 600 μL MeOH containing 0.1% formic acid and centrifuged (12,000 rpm, 5 min). The supernatants (600 μL) were collected and dried under nitrogen (Organomation, HSC-24A) then dissolved in 50 μL 50% MeOH. After centrifugation, supernatants (5 μL) were collected for LC−MS analysis. The pump flow rate of HPLC (LC-30AD, Shimadzu) was 0.5 mL/min, and the compounds were separated on an Agilent Eclipse plus C18 (4.6 mm × 150 mm, 3.5 μm). MeOH (A) and 0.1% formic acid water (B) are gradient elutions: 0−1.5 min, 15%−5% A; 1.5−3 min, 5%−60% A; 3−5 min, 60% A; 5−8 min, 60%−5% A. MS (ESI) spectrometry (AB API4000) equipped with an electrospray ionization source was used for detection. Generic parameter set: ion-transfer capillary temperature 500 °C, capillary voltage 4.5 kV, dwell time 100 ms, collision gas 8 psi of argon, GS1 40 psi of argon, GS2 60 psi of argon, and CUR 20 psi. Standard cures for **21b** and **21c** are $Y = 0.0035X + 0.0018$ ($R = 0.9986$, LLOQ = 2.24 pg/mL) and $Y = 0.0043X + 0.0064$ ($R = 0.9994$, LLOQ = 1.28 pg/mL), respectively. Analytes were performed by using multiple-reaction monitoring (MRM) mode. Retention time for internal standard, **21b** and **21c** are 2.84, 1.95 and 1.83 min, respectively. Pharmacokinetic parameters were calculated by noncompartmental methods using Phoenix WinNonlin.

4.2.10. Analysis of hypercholesterolemia models

Randomly grouped mice ($n = 6$) fed with medium fat diet (MFD) were treated by gavage once daily with compound **21b** (20 or 60 mg/kg) or 20 mg/kg lovastatin or combinations (20 mg/kg + 20 mg/kg) for 5 weeks. At 16 h post last gavage, blood (600 μL) was obtained by retro-orbital puncture, which was then centrifuged for 10 min (2000 rpm) to prepare serum for quantification of levels of serum TC, LDL-C and TG measured by automatic biochemical analyzer (C16000, Abbott). For liver collection, mice were sacrificed by cervical dislocation after blood collection. A small faction of livers was fixed with 10% formaldehyde saline for H&E staining ($n = 3$ per group) and Oil Red O. Meantime, another liver faction from randomly selected mice ($n = 3$ per group) were ground into nitrogen, then lysed for Western blot analysis as described detailed in the above section. The rest livers ($n = 6$ per group) were homogenized for the analysis of TC and TG levels. Survival, body weight and food intake were recorded weekly.

4.2.11. Statistical analysis

GraphPad Prism 7 was employed to perform all statistical analysis related to this work. Data are analyzed by one-way ANOVA multiple comparisons tests and expressed as the mean ± SD.

Acknowledgments

This work was supported by grants from Postdoctoral Research Foundation of China (2019M662007) and National Natural Science Foundation of China (81874286).

Author contributions

Hua Xiang and Guoshun Luo obtained the funding, designed the research and superintended the whole study. Guoshun Luo, Zhenbang Li and Xin Lin carried out the experiments and performed data analysis. Lizhe Zhu, Xinyu Li and Kun Xi designed and performed the molecular modeling. Yu Chen, Maoxu Xiao and Hanlin Wei participated part of the experiments. Guoshun Luo wrote the manuscript. Hua Xiang and Lizhe Zhu revised the manuscript. All the authors have read and approved the final manuscript.

Conflicts of interest

The authors have no conflicts of interest to declare.

Appendix A. Supporting information

Supporting information to this article can be found online at https://doi.org/10.1016/j.apsb.2020.11.001.

References

1. Virani SS, Alonso A, Benjamin EJ, Benjamin EJ, Bittencourt MS, Callaway CW, et al. Heart disease and stroke statistics-2020 update: a report from the american heart association. *Circulation* 2020;**141**:e139−596.
2. Leopold JA, Loscalzo J. Emerging role of precision medicine in cardiovascular disease. *Circ Res* 2018;**122**:1302−15.
3. Goldstein JL, Brown MS. A century of cholesterol and coronaries: from plaques to genes to statins. *Cell* 2015;**161**:161−72.
4. Goldstein JL, Brown MS. Regulation of the mevalonate pathway. *Nature* 1990;**343**:425−30.
5. Istvan ES, Deisenhofer J. Structural mechanism for statin inhibition of HMG-CoA reductase. *Science* 2002;**292**:1160−4.
6. Stancu C, Sima A. Statins: mechanism of action and effects. *J Cell Mol Med* 2001;**5**:378−87.
7. Sirtori CR. The pharmacology of statins. *Pharmacol Res* 2014;**88**:3−11.
8. Agouridis AP, Elisaf MS, Nair DR, Mikhailidis DP. All for statins and statins for all; an update. *Curr Pharmaceut Des* 2016;**22**:18−27.
9. Alonso R, Cuevas A, Cafferata A. Diagnosis and management of statin intolerance. *J Atherosclerosis Thromb* 2019;**26**:207−15.
10. Gislason GH, Rasmussen JN, Abildstrøm SZ, Gadsbøll N, Buch P, Friberg J, et al. Long-term compliance with beta-blockers,

angiotensin-converting enzyme inhibitors, and statins after acute myocardial infarction. *Eur Heart J* 2006;**27**:1153−8.
11. Ellis JJ, Erickson SR, Stevenson JG, Bernstein SJ, Stiles RA, Fendrick AM. Suboptimal statin adherence and discontinuation in primary and secondary prevention populations. *J Gen Intern Med* 2004;**19**:638−45.
12. Blackburn DF, Dobson RT, Blackburn JL, Wilson TW, Stang MR, Semchuk W. Adherence to statins, beta-blockers and angiotensin-converting enzyme inhibitors following a first cardiovascular event: a retrospective cohort study. *Can J Cardiol* 2005;**21**:485−8.
13. Schonewille M, de Boer JF, Mele L, Wolters H, Bloks VW, Wolters JC, et al. Statins increase hepatic cholesterol synthesis and stimulate fecal cholesterol elimination in mice. *J Lipid Res* 2016;**57**:1455−64.
14. Ness GC, Chambers CM, Lopez D. Atorvastatin action involves diminished recovery of hepatic HMG-CoA reductase activity. *J Lipid Res* 1988;**39**:75−84.
15. Burnett JR, Wilcox LJ, Telford DE, Kleinstiver SJ, Barrett PH, Newton RS, et al. The magnitude of decrease in hepatic very low density lipoprotein apolipoprotein B secretion is determined by the extent of 3-hydroxy-3-methylglutaryl coenzyme A reductase inhibition in miniature pigs. *Endocrinology* 1999;**140**:5293−302.
16. Reihner E, Rudling M, Stahlberg D, Berglund L, Ewerth S, Bjorkhem I, et al. Influence of pravastatin, a specific inhibitor of HMG-CoA reductase, on hepatic metabolism of cholesterol. *N Engl J Med* 1990;**323**:224−8.
17. Armitage J. The safety of statins in clinical practice. *Lancet* 2007;**370**:1781−90.
18. Rosenson RS, Baker SK, Jacobson TA, Kopecky SL, Parker BA. An assessment by the statin muscle safety task force: 2014 update. *J Clin Lipidol* 2014;**8**:S58−71.
19. Brown MS, Faust JR, Goldstein JL, Kaneko I, Endo A. Induction of 3-hydroxy-3-methylglutaryl coenzyme A reductase activity in human fibroblasts incubated with compactin (ML-236B), a competitive inhibitor of the reductase. *J Biol Chem* 1978;**253**:1121−8.
20. Luo J, Yang HY, Song BL. Mechanisms and regulation of cholesterol homeostasis. *Nat Rev Mol Cell Biol* 2020;**21**:225−45.
21. Brown MS, Goldstein JL. Multivalent feedback regulation of HMG CoA reductase, a control mechanism coordinating isoprenoid synthesis and cell growth. *J Lipid Res* 1980;**21**:505−17.
22. DeBose-Boyd RA. Feedback regulation of cholesterol synthesis: sterol-accelerated ubiquitination and degradation of HMG CoA reductase. *Cell Res* 2008;**18**:609−21.
23. Song BL, DeBose-Boyd RA. Ubiquitination of 3-hydroxy-3-methylglutaryl-CoA reductase in permeabilized cells mediated by cytosolic E1 and a putative membrane bound ubiquitin ligase. *J Biol Chem* 2004;**279**:28798−806.
24. Chen L, Ma MY, Sun M, Jiang LY, Zhao XT, Fang XX, et al. Endogenous sterol intermediates of the mevalonate pathway regulate HMGCR degradation and SREBP-2 processing. *J Lipid Res* 2019;**60**:1765−75.
25. Song BL, Javitt NB, DeBose-Boyd RA. Insig-mediated degradation of HMG CoA reductase stimulated by lanosterol, an intermediate in the synthesis of cholesterol. *Cell Metabol* 2005;**1**:179−89.
26. Johnson BM, DeBose-Boyd RA. Underlying mechanisms for sterol-induced ubiquitination and ER-associated degradation of HMG CoA reductase. *Semin Cell Dev Biol* 2018;**81**:121−8.
27. Jiang SY, Li H, Tang JJ, Wang J, Luo J, Liu B, et al. Discovery of a potent HMG-CoA reductase degrader that eliminates statin-induced reductase accumulation and lowers cholesterol. *Nat Commun* 2018;**9**:5138.
28. Pettersson M, Crews CM. Proteolysis targeting chimeras (PROTACs)—past, present and future. *Drug Discov Today Technol* 2019;**31**:15−27.
29. Neklesa TK, Winkler JD, Crews CM. Targeted protein degradation by PROTACs. *Pharmacol Ther* 2017;**174**:138−44.
30. Toure M, Crews CM. Small-molecule PROTACS: new approaches to protein degradation. *Angew Chem Int Ed Engl* 2016;**55**:1966−73.
31. Konstantinidou M, Li JY, Zhang BD, Wang ZF, Shaabani S, Brake TF, et al. PROTACs—a game-changing technology. *Expet Opin Drug Discov* 2019;**14**:1255−68.
32. Sun X, Gao HY, Yang YQ, He M, Wu Y, Song YG, et al. PROTACs: great opportunities for academia and industry. *Signal Transduct Target Ther* 2019;**4**:64.
33. Burslem GM, Crews CM. Proteolysis-targeting chimeras as therapeutics and tools for biological discovery. *Cell* 2020;**181**:102−14.
34. Gao H, Sun X, Rao Y. PROTAC technology: opportunities and challenges. *ACS Med Chem Lett* 2020;**11**:237−40.
35. Hu J, Hu B, Wang M, Xu F, Miao B, Yang CY, et al. Discovery of ERD-308 as a highly potent proteolysis targeting chimera (PROTAC) degrader of estrogen receptor (ER). *J Med Chem* 2019;**62**:1420−42.
36. Zhang Y, Loh C, Chen J, Mainolfi N. Targeted protein degradation mechanisms. *Drug Discov Today Technol* 2019;**31**:53−60.
37. Li X, Song Y. Proteolysis-targeting chimera (PROTAC) for targeted protein degradation and cancer therapy. *J Hematol Oncol* 2020;**13**:50.
38. Qian M, Yan F, Yuan T, Yang B, He Q, Zhu H. Targeting post-translational modification of transcription factors as cancer therapy. *Drug Discov Today* 2020;**25**:1502−12.
39. Khan S, He Y, Zhang X, Yuan YX, Pu SY, Kong QP, et al. Proteolysis targeting chimeras (PROTACs) as emerging anticancer therapeutics. *Oncogene* 2020;**39**:4909−24.
40. Liu J, Ma J, Liu Y, Xia J, Li YY, Wang ZP, et al. PROTACs: a novel strategy for cancer therapy. *Semin Canc Biol* 2020;**67**:171−9.
41. Winzker M, Friese A, Koch U, Janning P, Ziegler S, Waldmann H. Development of a PDEδ-targeting PROTACs that impair lipid metabolism. *Angew Chem Int Ed Engl* 2020;**59**:5595−601.
42. Cheng JF, Li Y, Wang X, Dong GQ, Sheng CQ. Discovery of novel PDEδ degraders for the treatment of KRAS mutant colorectal cancer. *J Med Chem* 2020;**63**:7892−905.
43. Cantrill C, Chaturvedi P, Rynn C, Petrig Schaffland J, Walter I, Wittwer MB. Fundamental aspects of DMPK optimization of targeted protein degraders. *Drug Discov Today* 2020;**25**:969−82.
44. Pike A, Williamson B, Harlfinger S, Martin S, McGinnity DF. Optimising proteolysis-targeting chimeras (PROTACs) for oral drug delivery: a drug metabolism and pharmacokinetics perspective. *Drug Discov Today* 2020;**25**:1793−800.
45. Churcher I. Protac-induced protein degradation in drug discovery: breaking the rules or just making new ones?. *J Med Chem* 2018;**61**:444−52.
46. Li MX, Yang YY, Zhao QY, Wu Y, Song L, Yang HY, et al. Degradation versus inhibition: development of proteolysis-targeting chimeras for overcoming statin-induced compensatory upregulation of 3-Hydroxy-3-methylglutaryl coenzyme A reductase. *J Med Chem* 2020;**63**:4908−28.
47. Chen JB, Chern TR, Wei TT, Chen CC, Lin JH, Fang JM. Design and synthesis of dual-action inhibitors targeting histone deacetylases and 3-hydroxy-3-methylglutaryl coenzyme A reductase for cancer treatment. *J Med Chem* 2013;**56**:3645−55.
48. Li YB, Yang JJ, Aguilar A, McEachern D, Przybranowski S, Liu L, et al. Discovery of MD-224 as a first-in-class, highly potent, and efficacious proteolysis targeting chimera murine double minute 2 degrader capable of achieving complete and durable tumor regression. *J Med Chem* 2019;**62**:448−66.
49. Peng LJ, Zhang ZS, Lei C, Li S, Zhang Z, Ren XM, et al. Identification of new small-molecule inducers of estrogen-related receptor α (ERRα) degradation. *ACS Med Chem Lett* 2019;**10**:767−72.
50. Bai N, Kirubakaran P, Karanicolas J. Rationalizing PROTAC-mediated ternary complex formation using Rosetta. *bioRxiv* 2020. Available from: https://doi.org/10.1101/2020.05.27.119347.
51. Drummond ML, Williams CI. *In Silico* modeling of PROTAC-mediated ternary complexes: validation and application. *J Chem Inf Model* 2019;**59**:1634−44.

52. Sircar A, Chaudhury S, Kilambi KP, Berrondo M, Gray JJ. A generalized approach to sampling backbone conformations with RosettaDock for CAPRI rounds 13-19. *Proteins* 2010;**78**:3115−23.
53. Feng D, Ge C, Tan ZY, Sun JG, Xie Y, et al. Isoflavones enhance pharmacokinetic exposure of active lovastatin acid *via* the upregulation of carboxylesterase in high-fat diet mice after oral administration of Xuezhikang capsules. *Acta Pharmacol Sin* 2018;**39**:1804−15.
54. Wang Y, Jiang X, Feng F, Liu W, Sun H. Degradation of proteins by PROTACs and other strategies. *Acta Pharm Sin B* 2020;**10**:207−38.
55. Tomoshige S, Ishikawa M. Recent progress in PROTACs and other chemical protein degradation technologies for the treatment of neurodegenerative disorders. *Angew Chem Int Ed Engl* 2021;**60**:3346−56.
56. Lin X, Xiang H, Luo GS. Targeting estrogen receptor α for degradation with PROTACs: a promising approach to overcome endocrine resistance. *Eur J Med Chem* 2020;**206**:112689.
57. Han X, Zhao L, Xiang W, Qin C, Miao B, Xu T, et al. Discovery of highly potent and efficient PROTAC degraders of androgen receptor (AR) by employing weak binding affinity VHL E3 ligase ligands. *J Med Chem* 2019;**62**:11218−31.
58. Sun Y, Zhao X, Ding N, Gao H, Wu Y, Yang Y, et al. PROTAC-induced BTK degradation as a novel therapy for mutated BTK C481S induced ibrutinib-resistant B-cell malignancies. *Cell Res* 2018;**28**:779−81.
59. Su S, Yang Z, Gao H, Yang H, Zhu S, An Z, et al. Potent and preferential degradation of CDK6 *via* proteolysis targeting chimera degraders. *J Med Chem* 2019;**62**:7575−82.
60. Crew AP, Raina K, Dong H, Qian Y, Wang J, Vigil D, et al. Identification and characterization of von Hippel-Lindau-recruiting proteolysis targeting chimeras (PROTACs) of TANK-binding kinase 1. *J Med Chem* 2018;**61**:583−98.
61. Qin C, Hu Y, Zhou B, Fernandez-Salas E, Yang CY, Liu L, et al. Discovery of QCA570 as an exceptionally potent and efficacious proteolysis targeting chimera (PROTAC) degrader of the bromodomain and extra-terminal (BET) proteins capable of inducing complete and durable tumor regression. *J Med Chem* 2018;**61**:6685−704.
62. Yang H, Lv W, He M, Deng H, Li H, Wu W, et al. Plasticity in designing PROTACs for selective and potent degradation of HDAC6. *Chem Commun* 2019;**55**:14848−51.
63. Bai L, Zhou B, Yang CY, Ji J, McEachern D, Przybranowski S, et al. Targeted degradation of BET proteins in triple-negative breast cancer. *Canc Res* 2017;**77**:2476.
64. Zhou H, Bai L, Xu R, Zhao Y, Chen J, McEachern D, et al. Structure-based discovery of SD-36 as a potent, selective, and efficacious PROTAC degrader of STAT3 protein. *J Med Chem* 2019;**62**:11280−300.